Check for updates

Original Article

Sugar palm (*Arenga pinnata (Wurmb.) Merr*) cellulosic fibre hierarchy: a comprehensive approach from macro to nano scale

Rushdan Ahmad Ilyas [a,b,*], Salit Mohd Sapuan [a,b,c,**], Rushdan Ibrahim [d], Hairul Abral [e], M.R. Ishak [f], E.S. Zainudin [a], Mochamad Asrofi [g], Mahmud Siti Nur Atikah [h], Muhammad Roslim Muhammad Huzaifah [a], Ali Mohd Radzi [a,i], Abdul Murat Noor Azammi [b,j], Mohd Adrinata Shaharuzaman [b,k,l], Norizan Mohd Nurazzi [a,b], Edi Syafri [m], Nasmi Herlina Sari [n], Mohd Nor Faiz Norrrahim [o], Ridhwan Jumaidin [p]

[a] Laboratory of Biocomposite Technology, Institute of Tropical Forestry and Forest Products, Universiti Putra Malaysia, 43400 UPM Serdang, Selangor, Malaysia
[b] Department of Mechanical and Manufacturing Engineering, Universiti Putra Malaysia, 43400 UPM Serdang, Selangor, Malaysia
[c] Advanced Engineering Materials and Composites Research Centre, Department of Mechanical and Manufacturing Engineering, Universiti Putra Malaysia, 43400 UPM Serdang, Selangor, Malaysia
[d] Pulp and Paper Branch, Forest Research Institute Malaysia, 52109 Kepong, Selangor, Malaysia
[e] Department of Mechanical Engineering, Andalas University, 25163 Padang, Sumatera Barat, Indonesia
[f] Department of Aerospace Engineering, Universiti Putra Malaysia, 43400 UPM Serdang, Selangor, Malaysia
[g] Laboratory of Material Testing, Department of Mechanical Engineering, University of Jember, Kampus Tegalboto, Jember 68121, East Java, Indonesia
[h] Department of Chemical and Environmental Engineering, Universiti Putra Malaysia, 43400 UPM Serdang, Selangor, Malaysia
[i] Faculty of Engineering and Technology, Linton Unversity Colledge, 71700 Mantin, Negeri Sembilan, Malaysia
[j] Automotive Department, Malaysia France Institute, University Kuala Lumpur, 43650 Bandar Baru Bangi, Selangor, Malaysia
[k] Faculty of Mechanical Engineering, Universiti Teknikal Malaysia Melaka, Hang Tuah Jaya, 76100 Durian Tunggal, Melaka, Malaysia
[l] Centre for Advanced Research on Energy, Universiti Teknikal Malaysia Melaka, Hang Tuah Jaya, 76100 Durian Tunggal, Melaka, Malaysia
[m] Department of Agricultural Technology, Politeknik Pertanian, Payakumbuh, Indonesia
[n] Mataram University, Jalan Majapahit No. 2 Mataram, West Nusa Tenggara, Indonesia
[o] Research Center for Chemical Defence (CHEMDEF), University Pertahanan Nasional Malaysia, Kem Perdana Sungai Besi, 57000 Kuala Lumpur, Malaysia
[p] Fakulti Teknologi Kejuruteraan Mekanikal dan Pembuatan, Universiti Teknikal Malaysia Melaka, Hang Tuah Jaya, 76100 Durian Tunggal, Melaka, Malaysia

* Corresponding author at: Laboratory of Biocomposite Technology, Institute of Tropical Forestry and Forest Products, Universiti Putra Malaysia, 43400 UPM Serdang, Selangor, Malaysia
** Corresponding author at: Laboratory of Biocomposite Technology, Institute of Tropical Forestry and Forest Products, Universiti Putra Malaysia, 43400 UPM Serdang, Selangor, Malaysia
E-mail: sapuan@upm.edu.my (S.M. Sapuan).

ABSTRACT

Sugar palm (*Arenga pinnata*) fibre is considered as a waste product of the agricultural industry. This paper is investigating the isolation of nanofibrillated cellulose from sugar palm fibres produced by a chemo-mechanical approach, thus opening a new way to utilize waste products more efficiently. Chemical pre-treatments, namely delignification and mercerization processes, were initially involved to extract the sugar palm cellulose. Then, mechanical pre-treatment was performed by passing the sugar palm cellulose through a refiner to avoid clogging in the subsequent process of high pressurized homogenization. Nanofibrillated cellulose was then characterized by its chemical properties (Fourier transform infrared spectroscopy), physical morphological properties (i.e. scanning electron microscopy, transmission electron microscopy, X-ray diffraction analysis), and thermogravimetric analysis. The nanofibres were attained at 500 bar for 15 cycles with 92% yield. The results showed that the average diameter and length of the nanofibrillated cellulose were found to be 5.5 ± 1.0 nm and several micrometres, respectively. They also displayed higher crystallinity (81.2%) and thermal stability compared to raw fibres, which served its purpose as an effective reinforcing material for use as bio-nanocomposites. The nanocellulose developed promises to be a very versatile material by having a huge potential in many applications, encompassing bio-packaging to scaffolds for tissue regeneration.

1. Introduction

Lignocellulosic nanomaterials have attracted interest from researchers as the alternative materials to replace synthetic materials, due to their sustainability and abundant source [1–3]. Nanofibrillated cellulose (NFC) from plant lignocellulose has particularly huge potential in many applications, from flexible food biodegradable packaging to scaffolds for tissue regeneration [1,4–7]. Nevertheless, the effectiveness of NFC production is still challenging with respect to commercial scale, high capacity, and energy consumption. Therefore, despite several methods for producing NFC that have been described by Khalil et al. [8], it is recently reported that all cellulosic fibre preparations involve some types of enzymatic or chemical pre-treatments prior to intensive mechanical disintegration. These enzymatic and chemical pre-treatments have been conducted to facilitate the disintegration of cellulose into nanofibrils, thus reducing the energy consumption. To date, several types of mechanical disintegration methods have been used to produce nanofibrillated cellulose, including high pressurized homogenization (HPH), microfluidization, ultrafine grinding or refining, cryocrushing in liquid nitrogen, high intensity ultrasonication (HIUS), and high speed blending [8–10]. HPH process includes passing cellulose slurry at a high pressure into a vessel through a very small nozzle. The fibres are then exposed to a large pressure drop with impact and shearing forces, as this valve opens and closes in rapid succession. The combination of impact and shearing forces promotes a high degree of nanofibrillation of the cellulose fibres, resulting in NFC [11]. According to Khalil et al. [8], HPH can be considered as an efficient method for refining of cellulosic fibres due to its simplicity, high efficiency, and non-requirement for organic solvents.

In the past decades, a wide range of agro-industrial residues had been used as the sources of NFC preparation, such as potato tuber cells [12], cassava bagasse [13], sugarcane bagasse, banana peels [14], wheat straw [15], rice straw [16], coir fibre [17], sugar beet [18], corn husk, and oat hulls [19]. In tropical countries, sugar palm fibres are presently categorized as waste products from sugar palm cultivation, whereby sugar palm is a multipurpose plant grown in these countries. The plant is a member of the *Palmae* family having almost 181 genera and an estimated number of 2600 species known globally. The fibres are mainly lignocellulosic and multicellular, which are found to have a high percentage of cellulose content [20–22]. Therefore, sugar palm fibres have a huge potential to be commercialized, specifically by producing highly valued nanomaterial products from agricultural waste. The utilization of this particular waste in bio-nanocomposite applications is one of the innovative ideas in solving the problem of underutilized renewable materials, hence generating a non-food market product for the agricultural industry [6,23–29]. It is well known from various literature that nanocellulose sourced from other conventional sources displays high stiffness and Young's modulus as high as 150 GPa [1]. Meanwhile, the tensile strength of the NFC is assumed to be approximately from 2 to 4 GPa [1]. Hence, an attempt has been made to isolate nanocellulose from sugar palm fibres and compare its properties with the values obtained so far from other conventional resources. This also offers an opportunity with regards to an effective disposal of the waste. Therefore, the present study aims to isolate NFC from an underutilized and waste raw material that is renewable, recyclable, inexpensive, and abundant in nature. So far, no work has been done regarding the extraction of NFC nanofibres from sugar palm fibres. Therefore, the current study was done and it had successfully isolated nanofibres

of NFC from sugar palm fibres through chemo-mechanical treatments, by using HPH and assisted with delignification, mercerization, and refining pre-treatments. The morphological, structural, physico-chemical, and thermal properties of the sugar palm NFC were subsequently analyzed using field emission scanning electron microscopy (FESEM), transmission electron microscopy (TEM), atomic force microscopy (AFM), Brunauer–Emmett–Teller (BET) analysis, degree of polymerization (DP), zeta potential, X-ray diffraction (XRD), Fourier transform infrared (FT-IR) spectroscopy, density, moisture content, and thermogravimetric analysis (TGA).

2. Materials and methods

2.1. Materials

Sugar palm fibres (SPF) were collected from Bahau District, Negeri Sembilan, Malaysia. The chemical reagents utilized included sodium chlorite, ethanoic acid and sodium hydroxide (purchased from Sigma–Aldrich, Malaysia).

2.2. Cellulose extraction

Sugar palm derived-cellulose was isolated from SPF by using delignification and mercerization processes [30]. The standard method of ASTM D1104-56 was applied to synthesize the holocellulose via delignification [31]. The resulting fibres were known as holocellulose, or sugar palm acid-treated fibres (SPATF). Afterwards, the holocellulose was converted to α-cellulose using ASTM D1103-60 standard [31]. The generated fibres were consequently known as sugar palm cellulose (SPC).

2.3. Isolation of sugar palm nanofibrillated cellulose (SPNFC)

2.3.1. Mechanical pre-treatment
A refining treatment prior to the HPH was required in order to enhance fibre accessibility and processing efficiency. Hence, the SPC was refined by 20,000 revolutions in a PFI-mill according to ISO 5264-2:2002 [32]. The process of refining the fibres resulted in the improvement of both external and internal fibrillation. Moreover, this process had improved the flow of fibre and avoided clogging during fluidization. The resultant fibres were known as sugar palm refined fibres (SPRF).

2.3.2. Mechanical high pressurized homogenization (HPH)
NFC from sugar palm fibre cellulose was isolated by the process of high pressurized homogenization (HPH). Typically, 1.8% fibre suspension in water was processed in a high pressurized homogenizer (GEA Niro Soavi, Panda NS1001L, Parma, Italy). The samples were passed 15 times through an intensifier pump that had increased the pump pressure, followed by the interaction chamber. This chamber had subsequently defibrillated the fibres by shear forces and impacts against the channel walls and colliding streams. Through the process, fibres were broken down from macro-sized structures to nano-sized structures, forming slurries of NFC. The high pressurized homogenizer was maintained to operate at 500 bar, whereas the fibrillation was conducted under neutral pH.

The temperature was not controlled, but fluidization was temporarily stopped when the temperature of the stock reached approximately 90 °C to prevent pump cavitation. The process was then continued when the samples had cooled to approximately 45 °C. Afterwards, ethylene gas at the temperature of −110 °C was used to freeze–dry the SPNFCs suspensions. Then, dried SPNFCs were collected and kept in a cool place for sample analysis.

2.4. Methods of characterization

2.4.1. Chemical composition determination
Treatment stages like raw fibres, acid-treated fibres, alkali-treated fibres and refined fibre were respectively considered for the determination of SPF's chemical compositions. Wise, Murphy, and D'Addieco method [33] was specifically used to determine the percentage of holocellulose. Meanwhile, the TAPPI standard techniques, namely T 222 (acid-insoluble lignin in wood and pulp) [34] and T 203 (alpha-, beta- and gamma-cellulose in pulp) [35] were simultaneously used for the determination of lignin (acid insoluble) and α-cellulose content in fibres.

2.4.2. Field emission scanning electron microscopy (FESEM)
The microstructure and nanostructure topography of the longitudinal cross section of SPFs, treated fibres, and SPNFCs were visualized with the aid of the FEI NOVA NanoSEM 230 machine (FEI, Brno-Černovice, Czech Republic), which possessed 3 kV accelerating voltage. A precautionary step to avoid over-charging was performed by coating the samples with gold.

2.4.3. Transmission electron microscopy (TEM)
TEM analysis was used to view the nanostructural images of the SPNFCs using a Philips Tecnai 20 machine with 200 kV acceleration voltage. Initially, dried SPNFCs were dispersed in distilled water and sonicated for 10 min to generate the SPNFCs' suspension. Afterwards, a drop of SPNFCs suspension was mounted on a carbon-coated metallic copper grid and was left to dry at room temperature.

2.4.4. Atomic force microscopy (AFM)
The AFM analysis was performed by using dimension edge with high-performance AFM tool (Bruker, Santa Barbara, CA, USA) in assistance of a software known as Bruker Nanoscope analysis (Version 1.7). It functioned using the Peak/Force tapping mode with a single controller (Nanoscope V from Bruker) for the estimation of the SPNFCs' thickness. A drop of SPNFCs suspension was dropped on the surface of an optical glass slide and was left to air dry. Then, the SPNFCs samples were scanned at room temperature and within controlled relative humidity in the tapping mode of the machine with OMCL-AC160TA standard Si probes (radius of tip less than 10 nm, spring constant of 2.98 N/m and resonant frequency of ∼310 kHz) under a scan rate of 1 Hz.

2.4.5. Yield
Solid content (Sc) about 0.2% was diluted with distilled water and centrifuged at 4500 rpm for 20 min before being dried to

a constant weight at 90 °C in a halogen desiccator. The yield was then calculated using Eq. (1), where %Sc was solid content percentage. The results represented the average values of three replicates.

$$Yield\% = \left(1 - \frac{weight\ of\ dried\ sediment}{weight\ of\ diluted\ sample \times \%Sc}\right) \times 100 \qquad (1)$$

2.4.6. Density

Gas intrusion under helium (He) gas flow and aided by an AccuPyc1340 pycnometer (Micromeritics Instrument Corporation, Norcross, GA, USA) was used to identify the samples' densities. The samples of SPFs, treated fibres and SPNFCs, respectively, were oven-dried at a temperature of 105 °C for 24 h to eliminate the moisture within the fibres. Then, these oven-dried fibres were placed into the desiccator to prevent absorption of atmospheric moisture prior to their insertion into the pycnometer. Five replicates of measurements were subsequently performed at a temperature of 27 °C and the mean values were then evaluated.

2.4.7. Moisture content

The moisture content experiment was carried out using five (5) prepared samples. All samples were kept in the oven at a temperature of 105 °C for a period of 24 h. The initial weight of the samples prior to the oven-drying process, M_i (g) and the final weight after the process, M_f (g) were measured so as to evaluate the moisture content. The computation of the moisture content of the samples was done with the aid of Eq. (2):

$$Moisture\ content(\%) = \frac{M_i - M_f}{M_i} \times 100 \qquad (2)$$

2.4.8. Porosity and surface area measurements

The N_2 adsorption–desorption or Brunauer–Emmet–Teller (BET) technique at 77 K with employment of a porosity and surface area analyzer BELSorp Mini II (NIKKISO, Osaka, Japan) was used to measure the surface area, size of pores, and their respective distribution. With the aid of the vacuum operating condition of 105 °C temperature for a period of 10 h, the samples were degassed. BET equation aided relative P/P_o pressure range of 10–20 to 1 was used to attain specific surface areas from the linear portion of the isotherms. In the meantime, Barrett–Joyner–Halenda (BJH) technique was used to determine distribution of pore size from the adsorption branch of the isotherms. The amount adsorbed at a relative pressure of $P/P_o = 0.98$ was used to estimate the total pore volume.

2.4.9. Degree of polymerization (DP)

Degree of polymerizations (DP) of the various samples of fibre suspension, such as SPF, SPATF, SPC, SPRF and SPNFCs, were respectively resolved based on their intrinsic viscosity [η]. The TAPPI standard method T230 om-08 [36] and ISO 5351 [37] were employed in the viscosity measurement of the highlighted fibre suspensions' samples. The fibre suspension, copper (II) ethylenediamine (CED) solution and distilled water were mixed together in the ratio 0.01:1:1, respectively, with CED serving as the main dissolution agent. The resultant mixture was cautiously shaken to ensure complete dissolution of the fibre suspension. The viscosity determination was then performed using Ubbelohde viscometer tube (Type 231, PTA Laboratory Equipment, Vorchdorf, Austria) on the produced solution and the initial solvent at 25 °C. Similar determinations were also carried out on the other fibre samples in triplicates. The Mark–Houwink approach, as related in Eq. (3), was used in the computation of the molecular weight of treated fibres, where [η] is the intrinsic viscosity and M is the molecular weight. The constant values of α and K had values of 1 and 0.42 for CED solvent, respectively.

$$[\eta] = KM^a \qquad (3)$$

2.4.10. Fourier transform infrared (FT-IR) spectroscopy

The detection of possible changes in the existing sugar palm fibres' functional groups at different treatments was carried out with the aid of FT-IR spectroscopic measurements (Nicolet 6700 AEM, Thermo Nicolet Corporation, Madison, WI, USA) within the range of 500–4000 cm^{-1}. The samples were mixed with potassium bromide and pressed into thin transparent films that were then subjected to FT-IR analysis.

2.4.11. X-ray diffraction (XRD)

The investigation of the raw fibres, treated fibres and nanofibres X-ray diffraction was determined using Rigaku D/max 2500 X-ray powder diffractometer (Rigaku, Tokyo, Japan), equipped with CuKα radiation (λ = 0.1541 nm) in the 2θ range 5–50°. The crystallinity index of each fibre sample X_c, as depicted in Eq. (4), can be deduced from the empirical method reported by Asrofi et al. [38] where I_{am} and I_{002} are the peak intensities of the amorphous and crystalline materials, respectively.

$$X_c = \frac{I_{002} - I_{am}}{I_{002}} \times 100 \qquad (4)$$

2.4.12. Zeta potential

The determination of the SPNFCs' size along with the characterization of the nanofibre surface charge property was carried out with the aid of Zetasizer Nano-ZS (Malvern Instruments, Worcestershire, United Kingdom). Each fibre sample was diluted by ten-fold in distilled water to 1 ml total volume and then placed into a particle size analyzer at room temperature (25 °C). The analysis employed the electrophoretic mobility (μm/s) of the nanofibres, which was converted to zeta potential using an in-built software based on the Helmholtz–Smoluchowski equation.

2.4.13. Thermogravimetric analysis (TGA)

TGA analyzer was used to investigate the thermal stability of the fibres, with respect to weight loss due to increase in temperature. In order to investigate the thermal degradation of sugar palm fibres at varying fibre treatments, the operating conditions were commonly set at a range of temperature of 25–600 °C, with the aid of a dynamic nitrogen atmosphere, and 10 °C heating rate, as well as conducting the analysis by depositing the fibre samples in aluminium pans.

Fig. 1 – Photographs of (a) the sugar palm tree, (b) raw sugar palm fibres, (c) bleached fibres, (d) alkali-treated fibres, and (e) refined fibres.
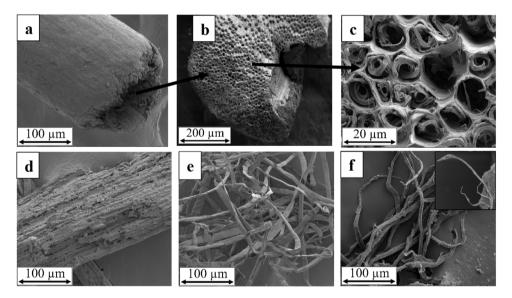

Fig. 2 – FE-SEM micrographs of (a) longitudinal section of raw sugar palm fibres, (b) cross section of raw sugar palm fibres, (c) primary, secondary cell wall and middle lamella, (d) bleached fibres, (e) alkali-treated fibres, and (f) refined fibres.

3. Results and discussion

3.1. Morphological study of sugar palm fibres and treated fibres

Fig. 1 displays the sugar palm tree and its fibres at different stages of treatment. The sugar palm fibres color changed from black (Fig. 1(b)) to brown after the bleaching treatment (Fig. 1(c)) and became white after alkali and refined treatments, respectively (Fig. 1(e)). FESEM micrographs of the cross and longitudinal section of the sugar palm fibres are represented in Fig. 2(a, b and g). The FESEM micrographs also displayed partial elimination of amorphous regions like hemicellulose, lignin, and pectin after the chemical treatment. These substances had acted as reinforcing components covering the fibre bundles.

The SPF longitudinal section surface morphology was found to be uneven, with pore-like spots that appeared in most regular intervals (Fig. 2(a)). These spots could also be found on coir fibre surfaces [39]. The clarity of the exterior surface of the fibres was a result of the removal of the waxy layer present on their exterior surface [40–42]. The mean diameter of the bleached fibres was reduced after the chemical treatment, from $212.01 \pm 2.17\,\mu m$ to $121.80 \pm 10.57\,\mu m$, which was attributable to the partial removal of lignin and

hemicellulose. After the alkali treatment (Fig. 2(e)), the fibre bundles were dispersed into individual micro-fibres with the diameter of $11.87 \pm 1.04\,\mu m$. In comparison, the diameter of raw sugar palm fibres doubled than that of bleached fibres, and was eighteen times larger than the alkali-treated fibres. In addition, the surface morphology of the raw SPC changed to smooth and groovy surfaces, along with parallel arrangement along the cellulose (Fig. 2(d)). Similar results were also reported by other authors, such as the average diameter of sisal cellulose ($13.5\,\mu m$) [43] and kenaf-derived cellulose ($13\,\mu m$) [44]. Similarly, microfibrillation of the sugar palm fibres after refining using PFI-mil is shown in (Fig. 2(f)). During the mechanical refining process, the microfibrils were pulled out from the fibres' cell wall due to the shearing action on their surfaces [45]. The sugar palm cellulose pulp was then beaten by the pressure present between the wall and the bar, in which a constant load was given to the pulp circulating between a stainless steel roll and cylindrical mill house. Their rotation with a constant difference in circumferential velocity had applied mechanical effects, such as shear and compression, thereby performing refining actions via frictional forces between the fibres. The microfibrils in this image displayed an average of $3.93 \pm 0.26\,\mu m$ in diameter, which was 55 times thinner than the raw sugar palm fibres. The refining process was commonly applied as a mechanical pre-treatment during the first stage of NFC production. It increased the fibre's specific surface and volume, as well as making the microfibrils more accessible for further mechanical treatment of HPH.

3.2. Chemical analysis of sugar palm fibres and treated fibres

Table 1 displays the chemical composition of sugar across different stages of treatment. After treating the fibres with NaClO$_2$ solution, the lignin content was reduced by 32.97%, whereas the cellulose was only reduced by about 12.79%. The alkali treatment affected the content of hemicellulose, which was reduced to 3.97%, while the cellulose increased by 25.66% that is almost two-fold compared to the acid-treatment fibres. This was caused by the cleavage of the ester-linked substances of hemicellulose [46]. In addition, the chemical treatment also allowed an increment in the surface area of the SPFs, thus making the polysaccharides defibrillating easily under high shear force. Meanwhile, the mechanical refining treatment, PFI-mill contributed to the defibrillation of SPFs by cleaving the inter-fibrillar hydrogen bonds between the nanofibril and caused the cellulose content to increase from 82.33% to 88.79%. This result was similar to the one reported earlier by

Hai et al. [47], who indicated that the PFI-mill refining process affected the cellulose content. The contents of cellulose, hemicellulose, and lignin after refined treatment were 88.79%, 0.04%, and 3.85%, respectively.

3.3. Isolation of SPNFCs

The nanocellulose suspension prepared from purified sugar palm fibres is shown in Fig. 3(a). The concentration of this suspension was 2 wt%. The FESEM observation and height of nanocellulose are shown in Fig. 3(b and c), respectively. TEM and AFM observations and their distribution of diameters are shown in Fig. 3(d and f) and Fig. 3(e and f), respectively. The defibrillation of sugar palm cellulose fibres to obtain nanoscale web-like termed as NFC was obtained by using a chemical pre-treatment and subsequent mechanical treatment of cellulose fibres. This consisted of pulp beating/refining (PFI-mill) and HPH processes. The yield of nanofibrils collected during the process of defibrillation was very high, with 92% nanofibrous elements having diameter values of $5.5 \pm 1.0\,nm$ (TEM) and $9 \pm 2\,nm$ (AFM) (Fig. 3(f and g)). The micrographs also resembled "noodle-like nanofibres" (Fig. 3(e)). The larger fibre diameter displayed in Fig. 3(e) may have resulted from a tip coardening effect, which was often associated with AFM. The height of the SPNFCs was recorded at 10.17 nm, whereby the value was close to the average nanofibre diameter ($9 \pm 2\,nm$) calculated from the AFM images. This obtained the yield of SPNFCs was in good agreement with the yield of eucalyptus wood (96%) and pine wood (88%) as reported by Besbes et al. [48]. Similar results of the diameters were reported by other authors on agro residue sources like banana (5 nm) [49] and flax fibres (5 nm) [50]. By comparing the microscopy images among TEM, FESEM and AFM, it could be deduced that TEM resulted in the clearest insight regarding the resultant NFCs morphology with widths that were the size of $5.5 \pm 1.0\,nm$. Additionally, it is well known that AFM is usually carried out for accurate measurement of the thickness of the nanofibres. Furthermore, the aqueous suspensions of NFCs were determined to be stable (Fig. 3(d)) due to the presence of evenly distributed negative charges, thus preventing agglomeration [51]. The negative charges induced electrostatic repulsion forces among the nanoparticles. This repulsive force kept the nanoparticles from collapsing into one another, thereby maintaining the stable suspension [52]. Meanwhile, the zeta potential analysis estimated the value of the negative charge on the SPNFCs to be −34.2 mV. These large negatively-charged zeta potential values were obtained due to the properties of the cellulose fibres, which contained —OH functional groups

Table 1 – Chemical constituent of sugar palm fibres at various stage of treatment.						
Samples	Cellulose (%)	Lignin (%)	Hemicellulose (%)	Holocellulose (%)	Ash (%)	Extractive (%)
SPF	43.88	33.24	7.24	51.12	1.01	2.73
SPATF	56.67	0.27	19.8	76.47	2.16	0.3
SPC	82.33	0.06	3.97	86.3	0.72	–
SPRF	88.79	0.04	3.85	94.64	0.74	–

SPF = raw sugar palm fibres; SPATF = sugar palm acid-treated fibres; SPC = sugar palm alkali-treated fibres; SPRF = sugar palm refined fibres.
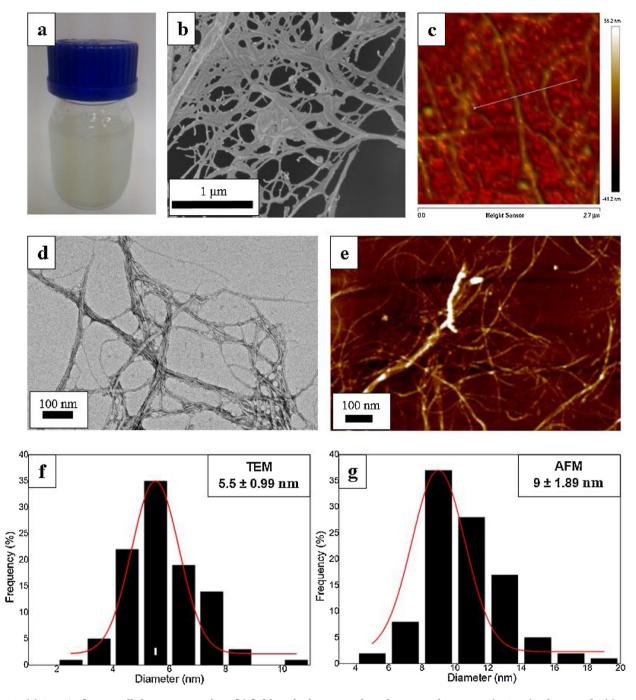
Fig. 3 – (a) 2 wt% of nanocellulose suspension, (b) field emission scanning electron microscopy (FESEM) micrograph, (c) height dimension of NFCs by means of atomic force microscopy (AFM) nanograph, (d) transmission electron microscopy (TEM) nanograph, (e) atomic force microscopy (AFM) nanograph, and (f and g) their diameter histograms based on TEM and AFM nanograph.

and gave the polymer its negative charge. The suspension of NFCs was considered stable as its absolute value was lesser than −30 mV and greater than 30 mV [53]. Therefore, all of these were considered as imperative qualities in the incorporation of NFCs as nano-reinforcement agents within the nanocomposites of a polymer.

3.4. Physical properties

Table 2 shows the physical properties (i.e. diameter, density, moisture content, degree of crystallinity, surface area, degree of polymerization and molecular weight) of untreated and treated fibres. It can be seen from Table 2 that the moisture

Table 2 – Physical properties of SPF [54], SPATF [54], SPC [54], SPRF, SPNFCs, and others nanofibres.

Samples	Diameter	Density (g/cm^{-3})	Moisture content (wt%)	X_c (%)	Surface area (m^2/g)	Pore volume (cm^3/g)	DP	M_w (g/mol)	Refs.
SPF	212.01 ± 2.17 μm	1.50	8.36 ± 0.0984	55.8	7.58	0.0607	–	–	[54]
SPATF	94.49 ± 0.03 μm	1.30 ± 0.0023	6.25 ± 0.0745	65.9	10.35	0.0678	2963.33	480,513.39	[54]
SPC	11.87 ± 1.04 μm	1.28 ± 0.0019	3.83 ± 0.1037	76.0	13.18	0.1950	946.48	153,458.51	[54]
SPRF	3.925 ± 0.26 μm	1.26 ± 0.001	3.08 ± 0.2231	77.7	13.66	0.2010	784.76	127,251.5	Current study
SPNFCs	5.5 ± 0.99 nm	1.1 ± 0.0026	12.855 ± 0.8912	81.2	14.01	0.2109	289.79	46,989	Current study
Eucalyptus urograndis NFC	30 nm	–	–	82	–	–	–	–	[65]
Kenaf bast fibre NFC	1–30 nm	–	–	81.5	–	–	–	–	[66]
Pineapple leaf NFC	30 nm	–	–	75.38	–	–	–	–	[67]

Results expressed as mean ± standard deviation.

content percentage had increased from raw sugar palm fibre (8.36 ± 0.10%) to SPNFCs (12.86 ± 0.89%). This may be attributed to the surface structure of cellulose that comprised of abundant hydroxyl groups known to be very sensitive to water molecules. The fibre surfaces were revealed to have abundant formations of hydrophilic ionic groups due to the treatments that were carried out during the process of bleaching, alkalinization, refining, and HPH. Besides, voids were created within the fibre structure, thereby led to fibres swell and to become well-separated. Therefore, the value of density decreased as the volume increased along with the loss in weight. In comparison with manmade fibres like glass fibre, aramid and carbon having density values of 2.5 g/cm^{-3}, 1.4 g/cm^{-3} and 1.7 g/cm^{-3}, respectively, SPNFC possessed a lower density value. Besides, the density of the fibre was also interrelated to its porosity and surface area; when the pore volume of the fibre increased, the fibre density would decrease. From the analysis, it could be concluded that all fibres displayed type IV isotherms accompanied by hysteresis loop, which were linked with capillary condensation that was taking place in mesopores (2–50 nm). Furthermore, the fibres also showed an increasing trend in cumulative pore volumes of sugar palm fibre (SPF) (0.061 cm^3/g) to SPNFC (0.211 cm^3/g). The increasing trend of cumulative pore volume was due to the fact that the SPF possessed closely aligned, rigid, and strong-bound building elements through hydrogen bonded cellulose structure, which was a result of the parting small interfacial spaces [55]. Through the mechanical treatment, opening of fibre bundles and defibrillation of individualized SPF that occurred was indirectly decreasing the size of the fibre from micro to nanoscale. This also resulted in an increase of the interfacial spaces between the nanofibrils. The BET surface area of the fibres also showed similar increasing trends as the cumulative pore volume. It was estimated that the surface area of SPNFCs was four times greater than SPF, which was higher and attributed to the nanosize SPNFCs as compared to macro-sized SPF.

Besides, Table 2 indicates that the DP and molecular weight of the fibres were reduced significantly from bleached fibre to SPNFCs, from 2963.33 to 289.79, and from 480,513.39 g/mol to 46,989 g/mol, respectively. The decreasing trend observed for the degree of fibre polymerization was attributed to the removal of lignin, hemicellulose, and inter-fibrillated hydrogen bonds between nanofibrils. This occurred due to the delignification, mercerization, refining, and HPH of the SPF. DP obtained for the SPNFCs was almost similar to the DP of beech wood (*Fagus sylvatica*) nanofibril (230) [56], higher than sugar beet pulp (120) [57], and lower than oil palm mesocarp microfibril (967) [58], soft wood of spruce (*Picea abies*) nanofibril (825), softwood (480) [59], wheat straw (*Triticum sp.*) nanofibril (674) [56], and empty palm fruit bunch (EPFB) (489 ± 23) [60].

3.5. FT-IR spectroscopy analysis

Fig. 4 displays the FT-IR spectra of SPF, acid-treated fibres, alkali-treated fibres, refined fibres, and nanofibrillated cellulose (NFCs). The intense peaks at 3100–3700 cm^{-1} were assigned to the adsorbed water, which also depicted the presence of hydroxyl groups in all fibres. Besides, there were many hydrogen bonded networks or hydroxyl functional groups on the surface of NFCs, corresponding to the hydroxyl stretching
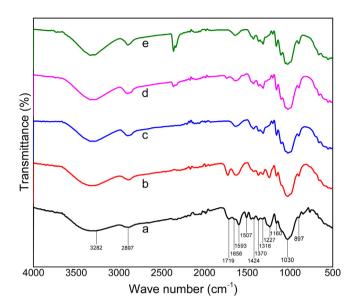

Fig. 4 – Fourier transform infrared spectroscopy of (a) raw sugar palm fibre [54], (b) bleached fibre [54], (c) alkali-treated fibre [54], (d) refined fibre, and (e) sugar palm nanofibrillated cellulose.

vibration at the 3100–3700 cm^{-1} region. These intense peaks remained in the NFCs peak after several treatments going on the raw SPF, whereas the intensity of the O—H groups peaked as the fibres were treated from raw fibres, bleached fibres, alkali treated fibres, refined fibres to NFCs. These occurrences were due to the large surface area exposed by the fibres, and resulting from the size reduction of the fibre dimension. Moreover, the presence of cellulose could be determined via the intense peak located at 897 cm^{-1} (C—H rocking vibrations), 1030 cm^{-1} (C—O stretching), 1160 cm^{-1} (C—O—C asymmetric valence vibration), 1316 cm^{-1} (C—H$_2$ rocking vibration), 1370 cm^{-1} (C—H$_2$ deformation vibration), and 1424 cm^{-1} [54].

The absorbance bands located at 1593 cm^{-1}, 1507 cm^{-1} and 1227 cm^{-1} were observed in the raw SPF, which indicated the C=C stretching of the aromatic rings of lignin [61]. However, these peaks were noted to disappear when the fibres underwent acid treatment of delignification process, signifying that such chemical process successfully eliminated lignin from the fibre composition. In addition, the absorbance peak of 1000–1300 cm^{-1} was observed to appear in all untreated and treated fibres, indicating the presence of C—O and C—H stretching groups [62].

3.6. X-ray diffraction measurements

Fig. 5 shows XRD patterns for sugar palm fibres at different stages of treatment. A well-defined mixture of cellulose I polymorph ($2\theta = 15°$ and $22.6°$) was observed in SPNFCs XRD pattern, with amorphous regions characterized at the small intensity peak at a $2\theta = 18°$. There was no presence of polymorphs of cellulose II ($2\theta = 12.3°$ and $22.1°$) in the X-ray diffraction. Cellulose I was the most stable structure compared to cellulose types II, III and IV [53]. The crystallinity index of fibres was observed to increase from 55.8% to 81.2%. The increment of the fibre crystallinity index was due to
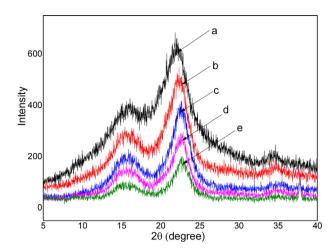
Fig. 5 – XRD arrays of (a) raw sugar palm fibres [54], (b) bleached fibres [54], (c) alkali-treated fibres [54], (d) refined fibres, and (e) SPNFCs.

the removal of non-cellulosic compounds of fibre (lignin and hemicellulose) by chemical and mechanical treatments. Furthermore, the humps were reduced after alkali-treatment showing that the amorphous chains had been arranged into crystalline regions. The larger crystallinity index can be known by observing the sharpness of the peak [63]. Similarly, it could also be comprehended from the diffractogram of cellulose, in which the sharpness in the edge of the diffractogram for the nanofibres had greatly increased. Moreover, the crystallinity index of SPNFCs was observed to be similar to kenaf bast fibre (*Hibiscus cannabinus v36*) (81.5%) [64], and higher than pine (75%) [48]. Thus, it could be concluded that the crystallinity values were different due to the plant's origins, as well as the types and variables of fibre purification used to disintegrate the fibres.

3.7. Thermogravimetric analysis (TGA)

Table 3 shows the thermogravimetry (TG) and derivative thermogravimetric (DTG) curve of untreated and treated fibres. Since the thermoplastic processing temperature will rise beyond 200 °C, therefore studying the thermal properties (i.e. TFA and DTG) of the natural fibres were crucial to determine their compatibility as nanofillers for biocomposite processing. Fig. 6 displays the TGA (i.e. TG-panel (i) and DTG-panel (ii)) outcomes for SPF, SPATF, SPC, SPRF and SPNFC fibres, respectively. The percentage of weight loss for all sugar palm fibres was

compared and displayed accordingly in Table 3. It was noted that the decomposition temperature of SPF had basically taken place in four (4) stages [54]. The first stage was referred to as the evaporation stage, which occurred in the temperature range of 45–123 °C and in which the moisture contained in the fibres was evaporated. The second stage was the decomposition stage occurring at around 220 °C to approximately 315 °C, in which the lignocellulosic components of hemicelluloses contained in the fibres were decomposed. Closely following this stage was the 3rd stage of cellulose decomposition, which was in the temperature range of 315 °C to ~400 °C, and followed by the fourth stage. The final stage witnessed the elimination of lignin in the temperature range of 165 °C to ~900 °C, and lastly, ash formation at 1723 °C.

The evaporation of moisture content in fibres within the temperature range of 29–42 °C marked the beginning of fibre weight loss and the weight reduction continued as the fibres were heated. The movement of water and volatile extractives that occurred may be a result of the water molecule migration, which also carried extractives from the internal part of the fibres to their external part (i.e. fibre surfaces) [65]. Furthermore, the evaporation of water molecules from the raw SPF and treated fibres took place at 196.56 °C and 134–189 °C, respectively (Fig. 6). The difference of the temperature may be perceived as an indicator of the varying moisture content within raw and treated SPF, accordingly. The highest moisture content (MC) was attained by raw fibre (10.38%) in comparison to the treated fibre. Upon treating the fibres, the MC decreased and led to correspondingly low weight loss. Such low weight losses may be adduced to the minimal loss of volatile extractives in the fibres, which was also linked to low heating temperature. The MC of the cell lumen and cell wall were equally small, but severe weight loss of approximately up to 70% might be attributable to the main components of the fibres (i.e. hemicellulose, cellulose and lignin). This was due to their role being the location where the decomposition process took place at temperature of 100 °C and above [65]. Besides, the weight loss of SPNFCs was higher than SPRF due to the surface structure of cellulose, which comprised of abundant hydroxyl groups known to be very sensitive to water molecules. The degradation of hemicellulose constituted as the second stage of the entire process. Usually, hemicellulose was readily converted into CO_2, CO, and some hydrocarbons at the low-temperature ranges of 220–315 °C. Therefore, the DTG curve of SPF fibre presented an initial weight loss that commenced at 210.58 °C before continuing to the highest temperature of 281 °C. These values were suggestive of low degradation temperature of lignin and hemicellulose [66].

Samples	Moisture evaporation			First stage decomposition			Second stage decomposition			Char yield, W (%)	Ref.
	T_{Onset} (°C)	T_{Max} (°C)	W_L (%)	T_{Onset} (°C)	T_{Max} (°C)	W_L (%)	T_{Onset} (°C)	T_{Max} (°C)	W_L (%)		[54]
Sugar palm fibres	41.73	106.78	10.38	210.58	281	15.13	308.05	345.45	43.76	30.73	[54]
Bleached fibres	42.37	103.74	9.87	195.66	271.56	15.24	288.35	324.44	52.39	22.5	[54]
Alkali-treated fibre	43.49	101.23	8.58	207.92	346.09	73.71	–	–	–	17.71	[54]
SPPFI	33.60	104.93	7.6	204.29	345.77	76.35	–	–	–	14.86	Current study
SPNFCs	28.71	102.80	8.94	192.71	347.30	72.44	–	–	–	17.17	Current study

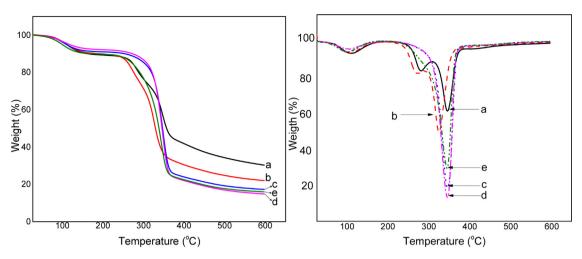Table 3 – Decomposition temperature of SPF[54], SPATF[54], SPC[54], SPRF, and SPNFCs.

Fig. 6 – (i) Thermogravimetry (TG) and (ii) derivative thermogravimetric (DTG) curves for (a) raw sugar palm fibres [54], (b) bleached fibres [54], (c) alkali-treated fibres [54], (d) refined fibre and (e) SPNFCs.

Similarly, the delignification process encouraged the expulsion of fibre components, such as lignin, hemicelluloses, and waxes, thereby giving rise to high surface having well-defined fibril aggregates. Meanwhile, the low percent composition of lignin in the SPATF fibres compared to that of raw SPF as revealed in Table 3 was suggestive of a reduction in the value of the temperature of acid-treated fibres. Additionally, lignin is a very difficult component to degrade (160–900 °C) in the raw SPFs, which functioned as the agent of stiffness to the cell wall and cemented individual cells together in the middle lamella region of the fibres [65]. Following the elimination of the lignin from the raw SPFs via the bleaching process, the left-over chemical substances in the fibres were mainly composed of hemicellulose and cellulose. Therefore, the low degradation temperature of hemicellulose (220–315 °C) in comparison to other macromolecules like cellulose and lignin suggested for its readily decomposing function within the alkaline medium. The small peaks that appeared at 281 and 271.56 °C in the neighbourhood of the main peak during the degradation of (a) SPF, and (b) SPATF, respectively, may be ascribed to the presence of hemicellulose and lignin. However, these peaks were not visible in the SPATF and SPNFCs. The weight losses were also observed to be much more progressive in the raw SPFs than that of the treated fibres. Besides, the observed shoulder in DTG analysis at around 300 °C for the raw SPFs was missing in the alkali-treated fibres, indicating the partial removal of the hemicellulose [46].

The degradation of cellulose took place at the third stage, which commenced at the temperature range of 315–400 °C [67]. Furthermore, alkali-treated fibres (c) unveiled a rise in the weight loss during the first degradation ($W_L = 73.71\%$; $T_{Max} = 346.09$) and second degradation ($W_L = 43.76\%$; $T_{Max} = 345.45$), in comparison with the raw SPFs and the second degradation of SPATF ($W_L = 52.39\%$; $T_{Max} = 324.44$). The alkali-treated fibres produced cellulose fibres with a high decomposition temperature at around 346 °C. Such outcome may be attributed to the partial elimination of hemicellulose and lignin during the bleaching process, as shown in Table 1. This result also verified cellulose's capability to withstand high-temperature deformation

process. Meanwhile, the alkali-treatment stage involved the oxidation of lignin and hemicellulose to yield simple sugars, which subsequently released the cellulose fibres [40,41,68]. The decomposition temperature of treated fibres was around 200 °C, which was smaller than raw SPFs. Similar results were also reported on mulberry bark celluloses by Li et al. [69] and pure celluloses by Soares et al. [70]. The decomposition temperature decreased due to the removal of the lignin and the strongly binding macromolecule of the fibres, thus leaving behind the hemicellulose constituent after the chemical treatment of the fibres. Hemicellulose was often present between and within cellulose fibrils. Therefore, the relatively strong reinforcement between hemicellulose and cellulose fibril gave rise to the reduced cellulose fibril crystallinity, thus speeding the thermal degradation process. The thermal data in Table 3 reveals that SPRF had a low thermal decomposition (T_{max}) of 345.77 °C compared to the SPNFCs sample, attributable to the difference in crystalline organization. Meanwhile, SPNFCs displayed gradual thermal transitions in the temperature region of 190–380 °C, whereby it was fundamentally related to the cellulosic chain degradation. Similarly, the T_{max} of SPNFCs (347.40 °C) was greater than that of NFC extracted from commercialized MCC, as reported by Li et al. [71] and had obtained DTG peak temperature T_{max} of 238 °C. Thus, the obtained SPNFCs reaffirmed good thermal stability that was comparable to that of NFC obtained from eucalyptus pulp (307.9 °C), as per the investigations conducted by Wang et al. [72], respectively. Besides, these results may also be due to the highly crystalline organization of the treated fibres, which strengthened the fibres in withstanding severe processing conditions like high temperature. Besides, HPH process was successful in reducing the micro-size fibre chain into nano-size fibres with the application of high shear force on the fibres. Hence, the outcomes from this study confirmed that the SPNFCs displayed thermal property improvements for treated fibres in comparison with the untreated fibres. They consequently supported the nanofibre's suitability as reinforcing materials in the preparation of renewable biocomposites. Polymer biocomposites with high thermal property can be potentially utilized in various applications. The decomposition of lignin within

the fibres predominated the fourth stage, which was quite difficult, unlike the degradation of hemicellulose and cellulose. This was due to the wide range of temperature (160–900 °C) involved in the process, as lignin possessed rigid structure that supported plant fibres and bonded individual cells together in the middle lamella portion of the fibres. However, the decomposition of lignin took place at a rather low weight loss rate (<0.14 wt%/°C) from the ambient temperature to 900 °C [65]. Additionally, Fig. 6 also unveils the slight differences in the TG and DTG curves of the treated and untreated fibres. The second SPF curve shifted to the right upon comparison with the SPATF curve. Such observation may be due to the high content of lignin (33.24%) found in the SPF fibres compared with the SPATF (0.27–2.78%), which prevented the hemicellulose from being easily disintegrated.

The final degradation stage witnessed the process of oxidation and breaking down of the charred residues. These residues with DTG peak above 425 °C were converted to lower molecular weight gaseous products [66]. Following full disintegration of lignin, the remaining residue left was an inorganic material typically referred to as ash content or char residue. The inorganic substance that made up the char residue included silica (i.e. silicon dioxide, SiO_2), which was only decomposable at the elevated temperature of 1723 °C and above [65]. Nonetheless, the SPATF and SPC produced low weight residue compared to that of raw SPF due to the removal of hemicellulose and lignin constituents from both treated fibres. Similarly, the high residual weight of SPNFCs was likely due to the char formation from flame retardant compounds.

4. Conclusions

In this study, NFCs were successfully isolated from sugar palm fibre (*Arenga pinnata (Wurmb) Merr.*) using chemo-mechanical treatment. The average diameter and length of the NFCs were found to be 5.5 nm and several micrometres, respectively. Based on the chemical compositions of the SPF, SPATF, SPC, and SPRF samples, there were significant reduction in the lignin and hemicellulose contents after delignification, mercerization and refining treatments. The presence of cellulose could otherwise be determined through the intense peak located at 897 cm^{-1} (C—H rocking vibrations), 1030 cm^{-1} (C—O stretching), 1160 cm^{-1} (C—O—C asymmetric valence vibration), 1316 cm^{-1} (C—H$_2$ rocking vibration), 1370 cm^{-1} (C—H$_2$ deformation vibration), and 1424 cm^{-1}. Meanwhile, well-defined cellulose I polymorph peaks at $2\theta = 15°$ and 22.6° in the XRD patterns of NFCS indicated an increase of cellulose crystallinity degree. The crystallinity index of fibres was also observed to increase from 55.8% (SPF) to 81.2% (SPNFCs). Therefore, it could be concluded that chemical treatments (i.e. delignification and mercerization) followed with HPH were effective to isolate SPNFCs from sugar palm fibres with a high yield of 92%. In this work, a value had been added to the agro-waste material, apart from the generation of eco-friendly SPNFC nanofillers for diversified applications.

Conflicts of interest

The authors declare no conflicts of interest.

REFERENCES

[1] Ilyas RA, Sapuan SM, Sanyang ML, Ishak MR, Zainudin ES. Nanocrystalline cellulose as reinforcement for polymeric matrix nanocomposites and its potential applications: a review. Curr Anal Chem 2018;14:203–25, http://dx.doi.org/10.2174/1573411013666171003155624.

[2] Sapuan SM, Ilyas RA, Ishak MR, Leman Z, Huzaifah MRM, Ammar IM, et al. Development of sugar palm-based products: a community project. Sugar palm biofibers, biopolymers, and biocomposites. 1st ed. Boca Raton, FL: CRC Press/Taylor & Francis Group, 2018: CRC Press; 2018. p. 245–66, http://dx.doi.org/10.1201/9780429443923-12.

[3] Ilyas RA, Sapuan SM, Ishak MR, Zainudin ES, Atikah MSN. Nanocellulose reinforced starch polymer composites: a review of preparation, properties and application. In: Proceeding: 5th International Conference on Applied Sciences and Engineering (ICASEA, 2018). 2018. p. 325–41.

[4] Abitbol T, Rivkin A, Cao Y, Nevo Y, Abraham E, Ben-Shalom T, et al. Nanocellulose, a tiny fiber with huge applications. Curr Opin Biotechnol 2016;39:76–88, http://dx.doi.org/10.1016/j.copbio.2016.01.002.

[5] Abral H, Basri A, Muhammad F, Fernando Y, Hafizulhaq F, Mahardika M, et al. A simple method for improving the properties of the sago starch films prepared by using ultrasonication treatment. Food Hydrocoll 2019, http://dx.doi.org/10.1016/j.foodhyd.2019.02.012.

[6] Asrofi M, Abral H, Kasim A, Pratoto A, Mahardika M, Hafizulhaq F. Characterization of the sonicated yam bean starch bionanocomposites reinforced by nanocellulose water hyacinth fiber (WHF): the effect of various fiber loading. J Eng Sci Technol 2018;13:2700–15.

[7] Asrofi M, Abral H, Putra YK, Sapuan SM, Kim HJ. Effect of duration of sonication during gelatinization on properties of tapioca starch water hyacinth fiber biocomposite. Int J Biol Macromol 2018;108:167–76, http://dx.doi.org/10.1016/j.ijbiomac.2017.11.165.

[8] Khalil HPSA, Davoudpour Y, Islam MN, Mustapha A, Sudesh K, Dungani R, et al. Production and modification of nanofibrillated cellulose using various mechanical processes: a review. Carbohydr Polym 2014;99:649–65, http://dx.doi.org/10.1016/j.carbpol.2013.08.069.

[9] Syafri E, Kasim A, Abral H, Sudirman, Sulungbudi GT, Sanjay MR, et al. Synthesis and characterization of cellulose nanofibers (CNF) ramie reinforced cassava starch hybrid composites. Int J Biol Macromol 2018;120:578–86, http://dx.doi.org/10.1016/j.ijbiomac.2018.08.134.

[10] Syafri E, Kasim A, Abral H, Asben A. Cellulose nanofibers isolation and characterization from ramie using a chemical-ultrasonic treatment. J Nat Fibers 2018;00:1–11, http://dx.doi.org/10.1080/15440478.2018.1455073.

[11] Abdul Khalil HPS, Bhat AH, Yusra AFI. Green composites from sustainable cellulose nanofibrils: a review. Carbohydr

Polym 2012;87:963–79, http://dx.doi.org/10.1016/j.carbpol.2011.08.078.

[12] Dufresne A. Cellulose microfibrils from potato tuber cells: processing and characterization of starch–cellulose microfibril composites. Polymer 2000;76:2080–92, http://dx.doi.org/10.1002/(SICI)1097-4628(20000628)76:14<2080::AID-APP12>3.0.CO;2-U.

[13] Teixeira E, de M, Pasquini D, Curvelo AASS, Corradini E, Belgacem MN, et al. Cassava bagasse cellulose nanofibrils reinforced thermoplastic cassava starch. Carbohydr Polym 2009;78:422–31, http://dx.doi.org/10.1016/j.carbpol.2009.04.034.

[14] Pelissari FM, Andrade-Mahecha MM, Sobral PJ, do A, Menegalli FC. Nanocomposites based on banana starch reinforced with cellulose nanofibers isolated from banana peels. J Colloid Interface Sci 2017;505:154–67, http://dx.doi.org/10.1016/j.jcis.2017.05.106.

[15] Kaushik A, Singh M, Verma G. Green nanocomposites based on thermoplastic starch and steam exploded cellulose nanofibrils from wheat straw. Carbohydr Polym 2010;82:337–45, http://dx.doi.org/10.1016/j.carbpol.2010.04.063.

[16] Nasri-Nasrabadi B, Behzad T, Bagheri R. Preparation and characterization of cellulose nanofiber reinforced thermoplastic starch composites. Fibers Polym 2014;15:347–54, http://dx.doi.org/10.1007/s12221-014-0347-0.

[17] Abraham E, Deepa B, Pothen LA, Cintil J, Thomas S, John MJ, et al. Environmental friendly method for the extraction of coir fibre and isolation of nanofibre. Carbohydr Polym 2013;92:1477–83, http://dx.doi.org/10.1016/j.carbpol.2012.10.056.

[18] Li M, Wang LJ, Li D, Cheng YL, Adhikari B. Preparation and characterization of cellulose nanofibers from de-pectinated sugar beet pulp. Carbohydr Polym 2014;102:136–43, http://dx.doi.org/10.1016/j.carbpol.2013.11.021.

[19] Valdebenito F, Pereira M, Ciudad G, Azocar L, Briones R, Chinga-Carrasco G. On the nanofibrillation of corn husks and oat hulls fibres. Ind Crops Prod 2017;95: 528–34, http://dx.doi.org/10.1016/j.indcrop.2016.11.006.

[20] Sapuan SM, Ishak MR, Leman Z, Ilyas RA, Huzaifah MRM. Development of products from sugar palm trees (*Arenga Pinnata Wurb. Merr*): a community project. INTROPica; 2017. p. 12–3.

[21] Radzi AM, Sapuan SM, Jawaid M, Mansor MR. Influence of fibre contents on mechanical and thermal properties of roselle fibre reinforced polyurethane composites. Fibers Polym 2017;18:1353–8, http://dx.doi.org/10.1007/s12221-017-73118.

[22] Jumaidin R, Sapuan SM, Jawaid M, Ishak MR, Sahari J. Effect of seaweed on physical properties of thermoplastic sugar palm starch/agar composites. J Mech Eng Sci 2016;10:2214–25, http://dx.doi.org/10.15282/jmes.10.3.2016.1.0207.

[23] Sanyang ML, Ilyas RA, Sapuan SM, Jumaidin R. Sugar palm starch-based composites for packaging applications. In: Bionanocomposites for packaging applications. Cham: Springer International Publishing; 2018. p. 125–47, http://dx.doi.org/10.1007/978-3-319-9-6.67317.

[24] Ilyas RA, Sapuan SM, Ishak MR, Zainudin ES. Development and characterization of sugar palm nanocrystalline cellulose reinforced sugar palm starch bionanocomposites. Carbohydr Polym 2018;202:186–202, http://dx.doi.org/10.1016/j.carbpol.2018.09.002.

[25] Ilyas RA, Sapuan SM, Ishak MR, Zainudin ES. Sugar palm nanocrystalline cellulose reinforced sugar palm starch composite: degradation and water-barrier properties. IOP Conf Ser Mater Sci Eng 2018;368:012006, http://dx.doi.org/10.1088/1757-899X/368/1/012006.

[26] Ilyas RA, Sapuan SM, Sanyang ML, Ishak MR. Nanocrystalline cellulose reinforced starch-based nanocomposite: a review. 5th postgraduate seminar on natural fiber composites. Serdang, Selangor: Universiti Putra Malaysia; 2016. p. 82–7.

[27] Ilyas RA, Sapuan SM, Ishak MR, Zainudin ES, Atikah MSN. Characterization of sugar palm nanocellulose and its potential for reinforcement with a starch-based composite. Sugar palm biofibers, biopolymers, and biocomposites. 1st ed. Boca Raton, FL: CRC Press/Taylor & Francis Group, 2018: CRC Press; 2018. p. 189–220, http://dx.doi.org/10.1201/9780429443923-10.

[28] Ilyas RA, Sapuan SM, Ishak MR, Zainudin ES. Water transport properties of bio-nanocomposites reinforced by sugar palm (*Arenga Pinnata*) nanofibrillated cellulose. J Adv Res Fluid Mech Therm Sci J 2018;51:234–46.

[29] Ilyas RA, Sapuan SM, Ishak MR, Zainudin ES, Atikah MSN, Huzaifah MRM. Water barrier properties of biodegradable films reinforced with nanocellulose for food packaging application: a review. 6th Postgraduate Seminar on Natural Fiber Reinforced Polymer Composites 2018, Serdang, Selangor; 2018. p. 55–9.

[30] Ilyas RA, Sapuan SM, Ishak MR, Zainudin ES. Effect of delignification on the physical, thermal, chemical, and structural properties of sugar palm fibre. BioResources 2017;12:8734–54, http://dx.doi.org/10.15376/biores.12.4.8734-8754.

[31] Sanyang ML, Sapuan SM, Jawaid M, Ishak MR, Sahari J. Effect of sugar palm-derived cellulose reinforcement on the mechanical and water barrier properties of sugar palm starch biocomposite films. BioResources 2016;11:4134–45, http://dx.doi.org/10.15376/biores.11.2.4134-4145.

[32] ISO 5264-2. Pulps — laboratory beating — Part 2: PFI mill method; 2002.

[33] Wise LE, Murphy M, D'Addieco AA. Chlorite, holocellulose, its fractionation and bearing on summative wood analysis and on studies on the hemicellulose. Paper Trade J 1946;122:35–43.

[34] T 222 om-02. Acid-insoluble lignin in wood and pulp. Tappi 2006.

[35] T 203 cm-99. Alpha-, beta- and gamma-cellulose in pulp. Tappi 2009.

[36] T 230 om-08. Viscosity of pulp (capillary viscometer, method). Tappi 2013.

[37] ISO 5351:2004(E). Pulps — determination of limiting viscosity number in cupri-ethylenediamine (CED) solution. International Standard; 2004.

[38] Asrofi M, Abral H, Kasim A, Pratoto A, Mahardika M, Hafizulhaq F. Mechanical properties of a water hyacinth nanofiber cellulose reinforced thermoplastic starch bionanocomposite: effect of ultrasonic vibration during processing. Fibers 2018;6:40, http://dx.doi.org/10.3390/fib6020040.

[39] Ticoalu A, Aravinthan T, Cardona F. A review on the characteristics of gomuti fibre and its composites with thermoset resins. J Reinf Plast Compos 2013;32:124–36, http://dx.doi.org/10.1177/0731684412463109.

[40] Thakur MK, Gupta RK, Thakur VK. Surface modification of cellulose using silane coupling agent. Carbohydr Polym 2014;111:849–55, http://dx.doi.org/10.1016/j.carbpol.2014.05.041.

[41] Thakur VK, Singha AS, Thakur MK. Synthesis of natural cellulose-based graft copolymers using methyl methacrylate as an efficient monomer. Adv Polym Tech 2013;32:E741–8, http://dx.doi.org/10.1002/adv.21317.

[42] Thakur VK, Singha AS, Thakur MK. Biopolymers based green composites: mechanical, thermal and physico-chemical characterization. J Polym Environ 2012;20:412–21, http://dx.doi.org/10.1007/s10924-011-y-0389.

[43] Savastano H, Warden P, Coutts RS. Brazilian waste fibres as reinforcement for cement-based composites. Cem Concr Compos 2000;22:379–84, http://dx.doi.org/10.1016/S0958-9465(00)00034-2.

[44] Tawakkal ISM, Talib R, Abdan K, Ling CN. Mechanical and physical properties of kenaf-derived cellulose (KDC)-filled polylactic acid (PLA) composites. BioResources 2012;7:1643–55, http://dx.doi.org/10.15376/biores.7.2.1643-1655.

[45] Tonoli GHD, Joaquim AP, Arsène M-A, Bilba K, Savastano H. Performance and durability of cement based composites reinforced with refined sisal pulp. Mater Manuf Process 2007;22:149–56, http://dx.doi.org/10.1080/10426910601062065.

[46] Sheltami RM, Abdullah I, Ahmad I, Dufresne A, Kargarzadeh H. Extraction of cellulose nanocrystals from mengkuang leaves (*Pandanus tectorius*). Carbohydr Polym 2012;88:772–9, http://dx.doi.org/10.1016/j.carbpol.2012.01.062.

[47] Hai L, Van Park HJ, Seo YB. Effect of PFI mill and Valley beater refining on cellulose degree of polymerization, alpha cellulose contents, and crystallinity of wood and cotton fibers. J Korea Tech Assoc Pulp Paper Ind 2013;45:27–33, http://dx.doi.org/10.7584/ktappi.2013.45.4.027.

[48] Besbes I, Rei M, Boufi S. Nanofibrillated cellulose from Alfa, Eucalyptus and pine fibres: preparation, characteristics and reinforcing potential. Carbohydr Polym 2011;86:1198–206, http://dx.doi.org/10.1016/j.carbpol.2011.06.015.

[49] Zuluaga R, Putaux J-LL, Restrepo A, Mondragon I, Gañán P. Cellulose microfibrils from banana farming residues: isolation and characterization. Cellulose 2007;14:585–92, http://dx.doi.org/10.1007/s10570-007–z-9118.

[50] Bhatnagar A. Processing of cellulose nanofiber-reinforced composites. J Reinf Plast Compos 2005;24:1259–68, http://dx.doi.org/10.1177/0731684405049864.

[51] Börjesson M, Westman G. Crystalline nanocellulose—preparation, modification, and properties. Cellulose – fundamental aspects and current trends. InTech; 2015. p. 159–91, http://dx.doi.org/10.5772/61899.

[52] Bondeson D, Mathew A, Oksman K. Optimization of the isolation of nanocrystals from microcrystalline cellulose by acid hydrolysis. Cellulose 2006;13:171–80, http://dx.doi.org/10.1007/s10570-006-90614.

[53] Naduparambath S, Shaniba J, Balan S, Purushothaman AK. Isolation and characterisation of cellulose nanocrystals from sago seed shells. Carbohydr Polym 2018;180:13–20, http://dx.doi.org/10.1016/j.carbpol.2017.09.088.

[54] Ilyas RA, Sapuan SM, Ishak MR. Isolation and characterization of nanocrystalline cellulose from sugar palm fibres (*Arenga Pinnata*). Carbohydr Polym 2018;181:1038–51, http://dx.doi.org/10.1016/j.carbpol.2017.11.045.

[55] Lu P, Hsieh Y. Preparation and characterization of cellulose nanocrystals from rice straw. Carbohydr Polym 2012;87:564–73, http://dx.doi.org/10.1016/j.carbpol.2011.08.022.

[56] Zimmermann T, Bordeanu N, Strub E. Properties of nanofibrillated cellulose from different raw materials and its reinforcement potential. Carbohydr Polym 2010;79:1086–93, http://dx.doi.org/10.1016/j.carbpol.2009.10.045.

[57] Habibi Y, Vignon MR. Optimization of cellouronic acid synthesis by TEMPO-mediated oxidation of cellulose III from sugar beet pulp. Cellulose 2008;15:177–85, http://dx.doi.org/10.1007/s10570-007-z-9179.

[58] Yasim-Anuar TAT, Ariffin H, Norrrahim MNF, Hassan MA. Factors affecting spinnability of oil palm mesocarp fiber cellulose solution for the production of microfiber. Bioresources 2017;12:715–34.

[59] Henriksson M, Berglund LA. Structure and properties of cellulose nanocomposite films containing melamine formaldehyde. J Appl Polym Sci 2007;106:2817–24, http://dx.doi.org/10.1002/app.26946.

[60] Ferrer A, Filpponen I, Rodríguez A, Laine J, Rojas OJ. Valorization of residual empty palm fruit bunch fibers (EPFBF) by microfluidization: production of nanofibrillated cellulose and EPFBF nanopaper. Bioresour Technol 2012;125:249–55, http://dx.doi.org/10.1016/j.biortech.2012.08.108.

[61] Arya EN, Wang ZJ, Ward RK. Image watermarking in higher-order gradient domain. Advances in wavelet theory and their applications in Engineering, Physics and Technology. InTech; 2012, http://dx.doi.org/10.5772/35603.

[62] Faix O, Lin S, Dence C. Fourier transform infrared spectroscopy. In: Methods in lignin chemistry. Springer-Verlag; 1992. p. 83–109.

[63] Alemdar A, Sain M. Isolation and characterization of nanofibers from agricultural residues – wheat straw and soy hulls. Bioresour Technol 2008;99:1664–71, http://dx.doi.org/10.1016/j.biortech.2007.04.029.

[64] Karimi S, Tahir PM, Karimi A, Dufresne A, Abdulkhani A. Kenaf bast cellulosic fibers hierarchy: a comprehensive approach from micro to nano. Carbohydr Polym 2014;101:878–85, http://dx.doi.org/10.1016/j.carbpol.2013.09.106.

[65] Ishak MR, Sapuan SM, Leman Z, Rahman MZA, Anwar UMK. Characterization of sugar palm (*Arenga Pinnata*) fibres tensile and thermal properties. J Therm Anal Calorim 2012;109:981–9, http://dx.doi.org/10.1007/s10973-011-1785-1.

[66] Flauzino Neto WP, Silvério HA, Dantas NO, Pasquini D. Extraction and characterization of cellulose nanocrystals from agro-industrial residue – Soy hulls. Ind Crops Prod 2013;42:480–8, http://dx.doi.org/10.1016/j.indcrop.2012.06.041.

[67] Yang H, Yan R, Chen H, Lee DH, Zheng C. Characteristics of hemicellulose, cellulose and lignin pyrolysis. Fuel 2007;86:1781–8, http://dx.doi.org/10.1016/j.fuel.2006.12.013.

[68] Deepa B, Abraham E, Cherian BM, Bismarck A, Blaker JJ, Pothan LA, et al. Structure, morphology and thermal characteristics of banana nano fibers obtained by steam explosion. Bioresour Technol 2011;102:1988–97, http://dx.doi.org/10.1016/j.biortech.2010.09.030.

[69] Li R, Fei J, Cai Y, Li Y, Feng J, Yao J. Cellulose whiskers extracted from mulberry: a novel biomass production. Carbohydr Polym 2009;76:94–9, http://dx.doi.org/10.1016/j.carbpol.2008.09.034.

[70] Soares S, Camino G, Levchik S. Comparative study of the thermal decomposition of pure cellulose and pulp paper. Polym Degrad Stab 1995;49:275–83, http://dx.doi.org/10.1016/0141-3910(95)87009-1.

[71] Wang Y, Wei X, Li J, Wang F, Wang Q, Kong L. Homogeneous isolation of nanocellulose from cotton cellulose by high pressure homogenization. J Mater Sci Chem Eng 2013;1:49–52, http://dx.doi.org/10.4236/msce.2013.15010.

[72] Wang Y, Wei X, Li J, Wang F, Wang Q, Zhang Y, et al. Homogeneous isolation of nanocellulose from eucalyptus pulp by high pressure homogenization. Ind Crops Prod 2017;104:237–41, http://dx.doi.org/10.1016/j.indcrop.2017.04.032.